Published in final edited form as:
Mol Pharm. 2013 March 4; 10(3): 857–866. doi:10.1021/mp300468q.

Theranostic Magnetic Core–Plasmonic Shell Star Shape Nanoparticle for the Isolation of Targeted Rare Tumor Cells from Whole Blood, Fluorescence Imaging and Photothermal Destruction of Cancer

Zhen Fan, **Dulal Senapati**, **Anant Kumar Singh**, and **Paresh Chandra Ray**
Department of Chemistry, Jackson State University, Jackson, MS, USA, Fax: 601-979-3674

Paresh Chandra Ray: paresh.c.ray@jsums.edu

Abstract

Cancer is one of the most life-threatening diseases, which causes 7.6 million deaths and around 1 trillion dollars economic loss every year. Theranostic materials are expected to improve early detection and safe treatment through personalized medicine. Driven by the needs, we report the development of a theranostic plasmonic shell–magnetic core star shape nanomaterial based approaches for the targeted isolation of rare tumor cells from the whole blood sample, followed by diagnosis and photothermal destruction. Experimental data with whole blood sample spiked with SK-BR-3 cancer cell shows that Cy3 attached S6 aptamer conjugated theranostic plasmonic/magnetic nanoparticles can be used for fluorescence imaging and magnetic separation even in 0.001% mixtures. A targeted photothermal experiment using 1064 nm near IR light at 2–3 W/cm^2 for 10 minutes resulted selective irreparable cellular damage to most of the SK-BR-3 cancer cells. We discuss the possible mechanism and operating principle for the targeted imaging, separation, and photothermal destruction using theranostic magnetic/plasmonic nanotechnology. After the optimization of different parameters, this theranostic nanotechnology-driven assay could have enormous potential for applications as contrast agent and therapeutic actuators for cancer.

Keywords

Theranostic star shape nanoparticle; Magnetic separation of cancer cell from whole blood; Selective Cancer cell imaging; Photothermal killing

Introduction

Cancer presents a great challenge to the public health care and the global economy [1–5]. Mortality and morbidity due to cancer cost nearly 1 trillion dollars per year. As a result, scientists and medical professionals are working to develop new approach for early stage detection and noninvasive treatment [6–13]. One promising method, but in this moment in very infant stage, is to use nanomaterial as a contrast agent and therapeutic actuators [14–30]. Nanoparticle possesses unique optical, magnetic and photo thermal properties which can be exploited for selective detection and non-invasive photothermal therapeutic applications of cancer [31–41]. Very recently, both functionalities, “diagnostic & therapeutic” have begun to be combined within a single multifunctional nanomaterial, resulting in the development of “theranostic” nanoparticle[16,20–30]. Scientists are seeking now to find out how theranostic nanoparticle can be used as an alternative to independently administer diagnostic probes and

Correspondence to: Paresh Chandra Ray, paresh.c.ray@jsums.edu.

traditional cancer therapy strategies [16,20–30]. The ideal theranostic nanomaterial should posses several features such as (1) highly selective accumulation in the diseased tissue, (2) delivers selectively an effective therapeutic action and (3) be safe and undergo biodegradation with nontoxic byproducts. Effective theranostic material development is a critical multidisciplinary and interdisciplinary field of the 21st century early stage cancer detection and treatment. Driven by the need, here we report the isolation of targeted rare tumor cells from whole blood, imaging and photothermal destruction of cancer cells using theranostic magnetic core–plasmonic shell star shape nanoparticle.

Although circulating tumor cells (CTCs) were first described in 1869 [1], even now CTC can be detected only in advanced stage cancer patients [2–10]. Scientists believe that early detection of CTC is the key towards better cure rates of cancer [2–8]. Since CTCs are present at extremely low abundance, accounting for 1 to fewer cells in 10^5–10^6 peripheral blood mononuclear cells, it is a real challenge in the early detection [1–8]. An effective separation & enrichment is highly crucial for further diagnosis. Plasmonic gold nanoparticles and super paramagnetic iron oxide nanoparticles are highly promising therapeutic materials, as reported in last one decade[9–30,40–50]. Upon successful trials, they may be used as drugs in cancer imaging & photothermal therapy. Due to the high transmission rate through biological tissues, gold nanoparticles of different sizes and shapes with optical properties tunable in the near-infrared (NIR) region are very useful for cancer imaging.[32–37,50–59]. In addition, gold nanoparticles have strong ability to generate high temperatures at the desired site, which is known as “optical nano heater” [32–37,50–59]. Due to all the above excellent properties and the lack of toxicity, perhaps the greatest promise of plasmonic gold nanotechnology in medicine will be its use in the early detection and therapeutic challenges of cancer. On the other hand, magnetic nanoparticles have been proved to be a highly promising candidate for magnetic resonance imaging (MRI) and biological separation.[18–40, 8–17, 45–60] Similarly, magnetic nanoparticles can also be used as “localized magnetic nano heater” in the presence of a strong magnetic field.[18–30] These above facts clearly indicate that the integration of magnetic and plasmonic functions can result in a perfect “theranostic” material. Theranostic nanoparticle developed by our group will have several advantages for its use as a medicine for cancer, as we have discussed below. Plasmonic gold coating on magnetic nanoparticles will be very useful for stabilizing high-magnetic-moment nanoparticles in corrosive biological conditions in the human body. Gold coating will eliminate the toxicity of iron nanoparticle. It will allow the conjugation of bio-recognition agent through the well-understood chemistry of Au-S. On the other hand, magnetic core will have high demand for circulating tumor cells separation & enrichment, from a complex mixture of heterogeneous cells in blood samples in “personalized medicine.” Also, plasmonic shell will be used as a photothermal material for the hyperthermic destruction of cancer using NIR light.

To demonstrate that our threanostic star shape nanoparticles can be used in CTC analysis in the settings close to clinical diagnosis, well-characterized SK-BR-3 human breast cancer cells were spiked at various cell densities into the suspensions of citrated whole rabbit blood, purchased from Colorado Serum Company. We have demonstrated that threanostic magnetic-plasmonic star shape nanoparticles developed by our group are capable of isolating rare cancer cells from whole blood sample, followed by imaging and photothermal destruction. We have used the SK-BR-3 human breast cancer cell line, which over-expresses the epithermal growth factor receptor HER2/c-erb-2/Neu (HER-2) on the cell surface [8,13]. Using an enzyme-linked immunosorbent assay kit, we found that the amount of HER2 in SK-BR-3 cells was 6.3×10^6/cell. No HER2 was found in rabbit whole blood cells. It is now known [61–63] that the interaction between nanomaterials and environmental biomolecules results in the formation of a biological corona on the nanoparticles surface. The proteins present in a biofluid can compete with NP surface to form a bio-nano interface. As a result,

in a biological fluid, proteins associate with nanoparticles could lead to a different cellular response than an uncoated particle. This response also will depend on the amount and the presentation of the proteins on their surface. Since S6 aptamer is known to exhibit highly specific targeting for the SK-BR-3 cell line *via* HER2, [13] we have used S6 aptamer-conjugated magnetic/plasmonic star shape nanoparticle for the specific targeting of SK-BR-3 cells.

Results and Discussions

We have synthesized theranostic core-shell star shape gold nanoparticle through a two-step process, using seed-mediated growth, as shown in Scheme 1. Details have been described in experimental section. TEM & SEM microscope images and UV-visible absorption spectrum were used to characterize the core-shell nanoparticles (as shown in Figure 1A–1D). Figure 1A shows the JEM-2100F transmission electron microscope (TEM) picture of iron nanoparticle and the size is about 10 nm. Figure 1D shows the absorption spectra of iron nanoparticle. Similarly, Figure 1B–IC show the TEM & SEM microscope images of magnetic core-plasmonic shell star shape nanoparticles, where the size is about 70 nm. Plasmon band around 1060 nm, as shown in Figure 1D, clearly shows the formation of gold shell. TEM and SEM microscope image shows clear spike, which indicates the formation of star shape nanoparticle.

For the magnetic separation of cancer cells from whole blood sample followed by fluorescence imaging, we first modified the magnetic/plasmonic nanoparticle surface with SK-BR-3 breast cancer-targeting S6 aptamer. Initially, to avoid nonspecific interaction with blood cells, star shape gold nanoparticle was coated by thiolated polyethylene glycol (HS-PEG) and then functionalized with aptamer. Details have been described in the experimental section. As shown in Scheme 1, in theranostic material, the magnetic core was used for cell isolation & enrichment. Cy3-modified S6 aptamers were attached to magnetic/plasmonic theranostic nanoparticles through -SH linkage for (a) specific SKBR-3 breast cancer cell recognition *via* the S6 aptamers and (b) fluorescence imaging using the Cy3 fluorescence probe.

Also, as shown in Scheme 1, in theranostic multifunctional nanoparticles, star shape gold plasmonic shells were used as both a photothermal agent and a nano platform. Also due to the surface roughness, the star shape magnetic-plasmonic particles certainly can enhance the protein corona attachment [64], which can enhance the cellular uptake and magnetic separation capability. The working principle for specific cancer cell separation from whole blood sample was based on the fact that in the presence of the SK-BR-3 cell line, S6 aptamer-conjugated theranostic nanoparticles were attached to the cancer cells due to the S6 aptamer–cancer cell interaction, as shown in Figure 2.

To demonstrate the CTC separation from whole blood sample, 0.001% of SK-BR-3 human breast cancer cells were spiked into the suspensions of citrated whole rabbit blood samples. Before spiking, we have used an enzyme-linked immunosorbent assay kit to determine the amount of HER2 in SK-BR-3 cells and blood cells. Our results show that the amount of HER2 in the SK-BR-3 cells was 6.3×10^6/cell, whereas no HER2 was found in blood cells. Then we have added 100 μL Cy3 modified S6 aptamer-conjugated magnetic/plasmonic nanoparticles. After 120 minutes incubation at room temperature under gentle shaking, cells attached with magnetic nanoparticles were separated by a magnet, as shown in Scheme 2. Then cells that bind with theranostic magnetic/plasmonic nanoparticles, as well as that did not bind with nanoparticles were characterized using TEM and enzyme-linked immunosorbent assay kits. Cells were also diagnosed using fluorescence imaging as shown in Scheme 2 & Figure 2. Using enzyme-linked immunosorbent assays, we found no HER2

in the fractions of cell suspensions that did not bind to magnetic/plasmonic nanoparticles. This data clearly show that spiked SK-BR-3 cells are attached with theranostic nanoparticle and were separated by a magnet. On the other hand, HER2 was present in the fractions of the cell suspension that had attached to the theranostic magnetic/plasmonic nanoparticles, indicating that the cells were human breast cancer SK-BR-3 cells. Our enzyme-linked immunosorbent assay experiments indicate that spiked rare tumor cell recovery was about 98%. As shown in Figures 2A–D, confocal fluorescence imaging showed that the targeted Cy3-bound aptamer-conjugated nanomaterials bound only to SK-BR-3 cells and not blood cells. Similarly, TEM images (Figures 2E, F) indicate that the targeted Cy3-bound aptamer-conjugated nanomaterials bound only to SK-BR-3 cells and not blood cells. All the above characterization results clearly show that S6 aptamer attached to magnetic/plasmonic nanoparticles is highly selective for binding with the SK-BR-3 cell line, which over-expresses HER2. Therefore, we believed that this theranostic nanoparticle can be used for imaging and the separation of CTC from whole blood sample even at 0.001% cell mixtures.

Next to demonstrate the selectivity of our assay, 0.001% of HER2-negative human prostate cancer LNCaP cell suspension were spiked into the suspensions of citrated whole rabbit blood samples. Before spiking, we have used an enzyme-linked immunosorbent assay kit to determine the amount of HER2 in LNCaP cells and blood cells. Our results show that no HER2 was found in blood cells as well as in LNCaP cells. Whereas, we found 6.6×10^6 PSMA/cell in LNCaP cell and no HER2 was found in blood cells. Then we have added 100 μL Cy3 modified S6 aptamer-conjugated magnetic/plasmonic nanoparticles in the blood sample. After 120 minutes incubation at room temperature under gentle shaking, cells attached to magnetic nanoparticles were separated by a magnet. Using enzyme-linked immunosorbent assay kits, we found that no PSMA was present in the magnetic separation portion. This clearly shows that Cy3 modified S6 aptamer-conjugated magnetic/plasmonic nanoparticles do not bind with HER2 negative LNCaP cells. TEM image & fluorescence microscope data also indicate that no cells are attached with Cy3 modified S6 aptamer-conjugated magnetic/plasmonic nanoparticles, which are separated by a magnet. Using enzyme-linked immunosorbent assays, we found PSMA in cell suspensions that did not bind to magnetic/plasmonic nanoparticles. All these experimental data clearly show that spiked LNCaP cells are not attached with theranostic nanoparticle and it indicates that our assay can be used for selective detection of SK-BR-3 cell from whole blood sample.

After successful targeted separation and fluorescence imaging, we have performed NIR irradiation experiments to determine whether theranostic magnetic/plasmonic nanoparticles can be used as a “optical nano heater” for photothermal killing for SK-BR-3 cancer cells. Gold nanoparticles are known to be capable of converting NIR light to vibrational energy, generating sufficient heat to kill cancer cells.[31–40,45–52]. As reported previously, when plasmonic nanoparticle are excited with near IR light,[31–40,45–52] the initial electronic excitation followed by relaxation give rise to a rapid increase in the surface temperature of the metal. This initial rapid heating will be cooled to equilibrium by energy exchange between the electrons and lattice. In the first several hundred picoseconds following excitation, the lattice will cool *via* phonons, resulting in local heating surrounding the nanostructure.[31–40] Local temperature increase produces sufficient heat for the destruction of the SK-BR-3 cancer cells. In the photothermal destruction experiment, we have used 1064 nm near IR light at 2–3 W/cm^2 for 10 minutes using a continuous wave Nd:YAG laser.

To determine the amount of cell death due to the hypothermia in the presence of 1064 nm light, we added trypan blue after NIR radiation exposure. Living cells cannot bind with trypan blue and are therefore colorless. On the other hand, dead cells bind with the blue dye. Therefore, cell viability can be qualitatively determined from the color of the cell monolayer. We have also used the MTT test to determine the number of live cells after

photothermal destruction process. As shown in Figure 3A, most of the cancer cells were dead after 10 minutes of the nanotherapy process for SK-BR-3 cells which were separated by the magnet. Bright-field inverted microscope images show that cancer cells were deformed during the nanotherapy process. The cell death following nanoparticle exposure to NIR radiation could be due to numerous factors including nanoparticle explosion, shock waves, bubble formation, and thermal disintegration.[31–40,45–52] Figure 3B shows the bright-field inverted microscope images of blood cells which are not separated by the magnet, after 20 minutes of exposure by 1064 nm light. Bright filed image clearly shows that our nanomaterial based photothermal killing is highly selective for the cells which were only attached with theranostic nanoparticle and separated by a magnet. As shown in Figure 3C, the time interval cell viability test indicated that within 10 minutes, most of the SK-BR-3 cancer cells, which are separated by a magnet were killed. On the other hand, cell viability was more than 97% in case of blood cells not separated by a magnet. This is because, the conjugation of theranostic magnetic/plasmonic nanoparticles with cancer cells is necessary for photothermal destruction using 1064-nm light. Cancer cells conjugated with magnetic/plasmonic nanoparticles should have strong absorption at the excitation wavelength, which is 1064 nm in our case. As shown in Figures 2, the conjugation of magnetic/plasmonic nanoparticles on cell membranes occurred only in HER2-positive SK-BR-3 cells. Therefore, the photothermal destruction effect should be highly efficient in the presence of SK-BR-3 cells. On the other hand, due to the lack of HER2 presence, blood cells are not conjugated with theranostic magnetic/plasmonic nanoparticles. As a result, they do not have any absorption at 1064 nm light. That is why the effective temperature increase in blood cells which are not conjugated with theranostic nanoparticle will be very little, which will be insufficient to kill these cells. Next, to understand how the temperature increases during photothermal destruction, we have also performed thermal imaging at 1-minute intervals during the therapy process using a MikroShot Camera. We found that the temperature increased to about 52°C when exposing theranostic magnetic/plasmonic nanoparticle-bound cancer cells to a 1064-nm laser at 2.5 W/cm^2. On the other hand, under the same conditions, the temperature increased to only 34°C for blood cells due to the absence of theranostic nanoparticles.

To understand how good the photothermal behavior of our synthesized theranostic iron magnetic core-star shape gold plasmonic shell nanoparticle, we have performed photothermal experiment with CNT attached gold nanoparticle using 1064 nm near IR light at 2–3 W/cm^2 for 20 minutes. For this purpose, we have first modified the hybrid nanoparticle with S6 aptamer and then conjugated with SK-BR-3 cells. As we have reported before [60] CNT attached gold nanoparticle hybrid exhibits very good photothermal behavior. Figure 3D shows that photothermal response for CNT/Gold hybrid is slightly better or comparable with our synthesized theranostic material. Though their photothermal responses are similar, due to the presence of magnetic core, currently reported theranostic material can be used for magnetic separation of cancer cell from whole blood sample. On the other hand, CNT/gold hybrid does not have any capability of magnetic cell separation from blood sample. As a result, iron magnetic core-star shape gold plasmonic shell nanoparticle reported by us will be a better theranostic material than CNT/gold hybrids.

Conclusions

In conclusion, in this article we have reported for the first time the development of theranostic iron magnetic core-star shape gold plasmonic shell nanoparticle for the targeted isolation of cancer cells from whole blood sample, followed by imaging and photothermal destruction. We found that S6 aptamer-conjugated theranostic magnetic/plasmonic nanoparticles are highly selective for binding to SK-BR-3 cells, which over-express HER2. Experimental data with whole blood sample spiked with SK-BR-3 cancer cell clearly

demonstrate that Cy3 attached S6 aptamer conjugated theranostic plasmonic/magnetic nanoparticles can be used for fluorescence imaging and magnetic separation even in 0.001% mixtures. Since circulating tumor cells are rare and accounts for 1 or fewer cells in 10^5–10^6 peripheral blood mononuclear cells, our reported star shape theranostic material can be useful for separation and initial enrichment for circulating tumor cells from clinical sample. We have also demonstrated that irradiation of near IR 1064 nm light on cancerous cells bound to S6 aptamer-conjugated magnetic/plasmonic nanoparticles, it selectively kills most of the cancer cells within 10 minutes. The localized heating that occurs due to the absorption of 1064-nm continuous NIR irradiation is able to cause irreparable cellular damage. This theranostic magnetic core–plasmonic shell nanotechnology-based assay is rapid; it only takes about 40 minutes from cancer cell binding to isolation and cell destruction. Even though the star shape theranostic magnetic/plasmonic nanoparticles have demonstrated promising results for cancer isolation form whole blood sample, fluorescence imaging and therapy, it is only fair to admit that we are at a relatively early stage of development. Another important factor need to be considered is that, the cell "vision" effect, which is recognized as a crucial factor for the safe design of any type of nanoparticles [65]. As a result, the impact of exactly the same nanomaterials on various cells can be significantly different and could not be assumed for other cells. Thus, what the cell "sees", when it is faced with nanomaterials, is most likely dependent on the cell type.

Experimental Section

Materials

Hydrogen tetrachloroaurate ($HAuCl_4.3H_2O$), cetyltrimethylammonium bromide (CTAB), $NaBH_4$, sodium citrate, iron chloride, were purchased from Sigma-Aldrich and used without further purification. Citrated whole rabbit blood was purchased from Colorado Serum Company (Denver, CO). The human breast cancer and growth media, phosphate buffered saline, trypsin, and fetal bovine serum were purchased from the American Type Culture Collection (ATCC, Rockville, MD).

Synthesis of theranostic magnetic core-star shape gold shell nanoparticle

We have synthesized iron nanoparticle magnetic core-popcorn shape gold shell nanoparticle through a two-step process, using seed-mediated growth, as shown in Figure 1A. In the first step, very small spherical iron nanoparticles were synthesized using tri-sodium citrate as a stabilizer and sodium borohydride as a strong reducing agent. For this purpose, we have added 2.5M $NaBH_4$ aqueous solution into a $FeCl_3$ deionized (DI) water drop-wise. And then we added 0.25mM tri-sodium citrate (TSC) aqueous solution at room temperature with vigorous stirring. TSC helps the formation of iron nanocrystals through the nucleation-growth pathway. Black powder was produced immediately. After 1 hour stirring, iron nanoparticles were separated and washed with DI water and ethanol by using a magnet. After that, we have dried the black powder in the N_2 atmosphere at room temperature. Figure 1A shows the JEM-2100F transmission electron microscope (TEM) picture of iron nanoparticle and the size is about 10 nm. Figure 1D shows the absorption spectra of ferric chloride and iron nanoparticle.

In the second step, star shaped magnetic nanoparticle was synthesized using the seed mediated growth procedure in the presence of cetyltrimethylammonium bromide (CTAB). The iron nanoparticles (2 mg) were re-dispersed in 0.5 mL of an aqueous 2.5 mM sodium citrate solution and sonicated for 20 min to produce a dark brown suspension. 3.9 mL of 10 mM $HAuCl_4$ solution was injected into a freshly prepared 0.05M CTAB, 5 mL solution. After that 0.9 mL of 4mM $AgNO_3$ was added and mixed properly. Then the iron seed solution was added into the solution at one time immediately after sonication under strong

stirring. At last, 0.6 mL of 0.078M ascorbic acid solution was added slowly drop by drop. After adding ascorbic acid, the solution became clear and colorless. The reaction mixture was allowed to stand for 30 mins. During the reaction process, the solution temperature was kept at 35 °C to keep the activity of the reaction. Fresh synthesized star shaped gold coated iron magnetic nanoparticles were separated and washed with acetone, ethanol and DI water 9 times by using a magnet to remove the extra CTAB in the reaction mixture solution. TEM & Hitachi 5500 Ultra high-resolution SEM microscope and UV-visible absorption spectrum were used to characterize the core-shell nanoparticles (as shown in Figure 1). The particle size was around 70 nm. Plasmon band around 1060 nm, as shown in Figure 1D, clearly shows the formation of gold shell. TEM and SEM image show clear spikes, which indicate the formation of star shape nanoparticle.

Synthesis of aptamer-conjugated magnetic/plasmonic nanoparticles—Initially, to avoid nonspecific interaction with blood cells, star shape theranostic nanoparticle was coated by thiolated polyethylene glycol (HS-PEG). After PEGylation, thiol-modified Cy3-bound S6 aptamers were gradually exposed to theranostic magnetic core–star shape plasmonic shell nanoparticles in the presence of 0.1 M NaCl in a PBS buffer over a 16-hour period. To remove the unbound aptamers, we centrifuged the solution at 6,000 rpm for 20 minutes, and the precipitate was then re-dispersed in 2 mL buffer solution; we repeated this process 3 times. To measure the number of aptamer molecules in each theranostic plasmonic/magnetic nanoparticle, we performed fluorescence analyses after the addition of potassium cyanide. To measure the number of aptamer molecules in each gold nanoparticle, after conjugation, we treated the Cy3-bound S6 aptamer-conjugated theranostic nanoparticles with 10 μM potassium cyanide to oxidize them. After that, the solution containing the released Cy3-labeled aptamers was collected for fluorescence analysis. The amount of Cy3-labeled S6 aptamers was measured by fluorescence. By dividing the total number of Cy3-labeled S6 aptamers by the total number of nanoparticles, we estimated that there were about 100–120 aptamers per theranostic magnetic/plasmonic nanoparticle.

Cell culture and incubation with magnetic/plasmonic nanoparticles—Cancer cells were grown in a 5% CO_2 incubator at 37°C using RPMI-1640 medium (ATCC, Rockville, MD) supplemented with 10% premium fetal bovine serum (FBS) (Lonza, Walkersville, MD) and antibiotics (10 IU/mL penicillin G and streptomycin) in 75-cm^2 tissue culture flasks. An enzyme-linked immunosorbent assay kit was used to quantify HER2 in tested cells. The experimental results indicate that the amount of HER2 in SK-BR-3 cells was 6.3×10^6/cell. No HER2 was observed in the blood cells. At first 0.001% SK-BR-3 cancer cells were spiked into the whole blood sample and different numbers of cells were then immersed into the aptamer-conjugated magnetic/plasmonic nanoparticle solution at room temperature before performing the magnetic separation experiment. After magnetic separation, we performed TEM and fluorescence analyses (as shown in Figure 2).

To measure the number of nanoparticle attached to each SK-BR-3 cell, after magnetic separation, we treated the Cy3-bound S6 aptamer-conjugated theranostic nanoparticles attached with SK-BR-3 cell with 10 μM potassium cyanide to oxidize them. After that, the number of nanoparticle attached to the cells was estimated using fluorescence analysis. Similarly total number of cell separated by the magnet was estimated using enzyme-linked immunosorbent assays. By dividing the total number of nanoparticles by the total number of cells, we estimated that there were about 80–100 attached theranostic nanoparticle/cell.

Fluorescence analysis—After cell separation by magnet, we used an Olympus IX71 inverted confocal fluorescence microscope fitted with a SPOT Insight digital camera for fluorescence imaging.

Photothermal destruction—For the photothermal destruction experiments, we used a continuous-wavelength CW Nd:YAG laser operating at 1064 nm as an excitation light source for 10–20 minutes. Then, we used the MTT test to determine the amounts of live cells after the photothermal destruction process. For this purpose, cells were seeded in 96-well plates (well diameter, 6.4 mm) at a density of 1×10^5 cells/well and were allowed to attach for 24 hours at 37°C in a 5% CO_2 incubator before the treatment. The cell monolayers in the wells were repeatedly rinsed with PBS buffer after incubation to remove the nonspecifically adsorbed nanomaterial remaining in the medium. Then, the monolayers were exposed to the 1064-nm laser.

Determination of the percentage of live cells

Cell viability was also determined 1 hour after photothermal treatment using the 3-(4,5-dimethylthiazol-2-yl)-2,5-diphenyltetrazolium bromide (MTT) cell proliferation assay kit (ATCC CA# 30-1010k). In MTT test, the live cell counting is based on the enzymatic reduction of the tetrazolium salt in living, metabolically active cells but not in dead cells. MTT reaction was carried out in situ in multiwell plates. At the end, the reaction product, a purple-colored formazan soluble in dimethylsulfoxide, was measured by the spectrophotometric technique. The absorbance at 540 nm was recorded using Multiskan Ascent Plate Reader with the Ascent software (Labsystems).This experiment was repeated 5–6 times. The results are expressed as mean values.

Acknowledgments

Dr. Ray is grateful for NSF-PREM grant # DMR-0611539 for their generous funding for nanomaterial research and NIH-RCMI grant # 5G12RR013459 for core facilities.

References

1. Ashworth TR. A case of cancer in which cells similar to those in the tumors were seen in the blood after death. Aust Med J. 1869; 14:146.
2. Nagrath S, Sequist LV, Maheswaran S, Bell DW, Irimia D, Ulkus L, Smith MR, Kwak EL, Digumarthy S, Muzikansky A, Ryan P, Balis UJ, Tompkins RG, Haber DA, Toner M. Isolation of rare circulating tumour cells in cancer patients by microchip technology. Nature. 2007; 450:1235–U10. [PubMed: 18097410]
3. Yu M, Stott S, Toner M, Maheswaran S, Haber DA. Circulating Tumor Cells as Biomarkers in Prostate Cancer. J Cell Biol. 2011; 192:373–377. [PubMed: 21300848]
4. Talasaz AH, Powell AA, Huber DE, Berbee JG, Roh K-H, Yu W, Xiao W, Davis MM, Pease RF, Mindrinos MN, Jeffrey SS, Davis RW. Isolating highly enriched populations of circulating epithelial cells and other rare cells from blood using a magnetic sweeper device. Proc Natl Acad Sci. 2009; 106:3970–3975. [PubMed: 19234122]
5. Thomas Budd G. Let Me Do More Than Count the Ways: What Circulating Tumor Cells Can Tell Us about the Biology of Cancer. Mol Pharmaceutics. 2009; 6:1307–1310.
6. Adams AA, Okagbare PI, Feng J, Hupert ML, Patterson D, Göttert J, McCarley RL, Nikitopoulos D, Murphy MC, Soper SA. Highly Efficient Circulating Tumor Cell Isolation from Whole Blood and Label-Free Enumeration Using Polymer-Based Microfluidics with an Integrated Conductivity Sensor. J Am Chem Soc. 2008; 130:8633–8641. [PubMed: 18557614]
7. Wang S, Wang H, Jiao J, Chen K-J, Owens GE, Kamei K-i, Sun J, Sherman DJ, Behrenbruch CP, Wu H, Tseng H-R. Three-Dimensional Nanostructured Substrates toward Efficient Capture of Circulating Tumor Cells. Angew Chem, Int Ed. 2009; 48:8970–8973.
8. Fehm T, Becker S, Duerr-Stoerzer S, Sotlar K, Mueller V, Wallwiener D. Determination of HER2 status using both serum HER2 levels and circulating tumor cells in patients with recurrent breast cancer whose primary tumor was HER2 negative or of unknown HER2 status. Breast Cancer Res. 2007; 9:R74. [PubMed: 17963511]

9. Jokerst, Jesse V.; Gambhir, Sanjiv S. Molecular Imaging with Theranostic Nanoparticles. Acc Chem Res. 2011; 44:1050–1060. [PubMed: 21919457]
10. Meyer M, Dohmen C, Philipp A, Kiener D, Maiwald G, Scheu C, Ogris M, Wagner E. Synthesis and biological evaluation of a bioresponsive and endosomolytic siRNA-polymer conjugate. Mol Pharmaceutics. 2009; 6:752–762.
11. Park K, Lee S, Kang E, Kim K, Choi K, Kwon IC. New Generation of Multifunctional Nanoparticles for Cancer Imaging and therapy. Adv Funct Mater. 2009; 19:1553–1566.
12. Dobson J. Remote Control of Cellular Behavior with Magnetic Nanoparticles. Nat Nanotechnol. 2008; 3:139– 143. [PubMed: 18654485]
13. King SH, Huh YM, Kim S, Lee D-K. Isolation of RNA Aptamers Targeting HER-2-overexpressing Breast Cancer Cells Using Cell-SELEX. Bull Korean Chem Soc. 2009; 30:1827–1831.
14. Namiki Y, Namiki T, Yoshida H, Ishii Y, Tsubota A, Koido S, Nariai K, Mitsunaga M, Yanagisawa S, Kashiwagi H, Mabashi Y, et al. Novel Magnetic Crystal-Lipid Nanostructure for Magnetically Guided *In Vivo* Gene Delivery. Nat Nanotechnol. 2009; 4:598– 606. [PubMed: 19734934]
15. Zou P, Yu Y, Wang YA, Zhong Y, Welton A, GalbaÌn C, Wang S, Sun D. Superparamagnetic iron oxide nanotheranostics for targeted cancer cell imaging and pH-dependent intracellular drug release. Mol Pharmaceutics. 2010; 7:1974–1984.
16. Ma, Xiaowei; Zhao, Yuliang; Liang, Xing-Jie. Theranostic Nanoparticles Engineered for Clinic and Pharmaceutics. Acc Chem Res. 2011; 44:1114–1122. [PubMed: 21732606]
17. Davis ME. The first targeted delivery of siRNA in humans via a self-assembling, cyclodextrin polymer-based nanoparticle: from concept to clinic. Mol Pharmaceutics. 2009; 6:659– 668.
18. Galanzha EI, Shashkov EV, Kelly T, Kim J, Yang L, Zharov VP. *In Vivo* Magnetic Enrichment and Multiplex Photoacoustic Detection of Circulating Tumour Cells. Nat Nanotechnol. 2009; 4:855–860. [PubMed: 19915570]
19. Mannix RJ, Kumar S, Cassiola F, Montoya-Zavala M, Ingber DE. Nanomagnetic Actuation of Receptor-Mediated Signal Transduction. Nat Nanotechnol. 2008; 3:36–40. [PubMed: 18654448]
20. Bhojani, Mahaveer Swaroop; Van Dort, Marcian; Rehemtulla, Alnawaz; Brian, D. Ross, Targeted Imaging and Therapy of Brain Cancer Using Theranostic Nanoparticles. Mol Pharmaceutics. 2010; 7:1921–1929.
21. Yoo, Dongwon; Lee, Jae-Hyun; Shin, Tae-Hyun; Cheon, Jinwoo. Theranostic Magnetic Nanoparticles. Acc Chem Res. 2011; 44:863–874. [PubMed: 21823593]
22. Quan, Qimeng; Xie, Jin; Gao, Haokao; Yang, Min; Zhang, Fan; Liu, Gang; Lin, Xin; Wang, Andrew; Henry, S. Eden, Seulki Lee, Guixiang Zhang, and Xiaoyuan Chen, HSA Coated Iron Oxide Nanoparticles as Drug Delivery Vehicles for Cancer Therapy. Mol Pharmaceutics. 2011; 8:1669–1676.
23. Sanson C, Diou O, Thévenot J, Ibarboure Emmanuel, Soum Alain, Bru3let Annie, Miraux Sylvain, Thiaudière Eric, Tan Sisareuth, Brisson Alain, Dupuis Vincent, Sandre Olivier, Lecommandoux Sébastien. Doxorubicin Loaded Magnetic Polymersomes: Theranostic Nanocarriers for MR Imaging and Magneto-Chemotherapy. ACS Nano. 2011; 5:1122–1140. [PubMed: 21218795]
24. Marites P. Melancon, Min Zhou, and Chun Li, Cancer Theranostics with Near-Infrared Light-Activatable Multimodal Nanoparticles. Acc Chem Res. 2011; 44:947–956. [PubMed: 21848277]
25. Duncan R, Gaspar R. Nanomedicine(s) under the Microscope. Mol Pharmaceutics. 2011; 8:2101–2141.
26. Perry, Jillian L.; Herlihy, Kevin P.; Napier, Mary E.; DeSimone, Joseph M. PRINT: A Novel Platform Toward Shape and Size Specific Nanoparticle Theranostics. Acc Chem Res. 2011; 44:990–998. [PubMed: 21809808]
27. Kim B, Schmieder AH, Stacy AJ, Williams TA, Pan D. Sensitive Biological Detection with a Soluble and Stable Polymeric Paramagnetic Nanocluster. J Am Chem Soc. 2012; 134:10377–10380. [PubMed: 22693958]
28. Bardhan R, Lal S, Joshi A, Halas NJ. Theranostic Nanoshells: From Probe Design to Imaging and Treatment of Cancer. Acc Chem Res. 2011; 44:936–946. [PubMed: 21612199]

29. Pan D, Caruthers SD, Hu G, Senpan A, Scott MJ, Gaffney PJ, Wickline SA, Lanza GM. Ligand-Directed Nanobialys as Theranostic Agent for Drug Delivery and Manganese-Based Magnetic Resonance Imaging of Vascular Targets. J Am Chem Soc. 2008; 130:9186–9187. [PubMed: 18572935]
30. Huschka R, Neumann O, Barhoumi A, Halas NJ. Visualizing light-triggered release of molecules inside living cells. Nano Lett. 2010; 10:4117–4122. [PubMed: 20857946]
31. Liu HL, Hua MY, Yang HW, Huang CY, Chu PC, Wu JS, Tseng IC, Wang JJ, Yen TC, Chen PY, Wei KC. Magnetic resonance monitoring of focused ultrasound/magnetic nanoparticle targeting delivery of therapeutic agents to the brain. Proc Natl Acad Sci USA. 2010; 107:15205–15210. [PubMed: 20696897]
32. Jain PK, Huang X, El-Sayed IH, El-Sayed MA. Noble metals on the nanoscale: optical and photothermal properties and some applications in imaging, sensing, biology, and medicine. Acc Chem Res. 2008; 41:1578–1586. [PubMed: 18447366]
33. Liong M, Lu J, Kovochich M, Xia T, Ruehm SG, Nel AE, Tamanoi F, Zink JI. Multifunctional inorganic nanoparticles for imaging, targeting, and drug delivery. ACS Nano. 2008; 2:889–896. [PubMed: 19206485]
34. Peer D, Karp JM, Hong S, Farokhzad OC, Margalit R, Langer R. Nanocarriers as an emerging platform for cancer therapy. Nat Nanotechnol. 2007; 2:751–760. [PubMed: 18654426]
35. Ray PC, Khan SA, Singh AK, Senapati D, Fan Z. Nanomaterial for Targeted Detection and Photothermal Killing of Bacteria. Chem Soc Rev. 2012; 41:3193–3209. [PubMed: 22331210]
36. Ray PC. Size and Shape Dependent Second Order Nonlinear Optical Properties of Nanomaterials and Their Application in Biological and Chemical Sensing. Chem Rev. 2010; 110:5332–5365. [PubMed: 20469927]
37. Huang X, El-Sayed IH, Qian W, El-Sayed MA. Cancer Cell Imaging and Photothermal Therapy in the Near-Infrared Region by Using Gold Nanorods. J Am Chem Soc. 2006:2115–2120. [PubMed: 16464114]
38. Kaittanis C, Santra S, Perez JM. Role of Nanoparticle Valency in the Nondestructive Magnetic-Relaxation-Mediated Detection and Magnetic Isolation of Cells in Complex Media. J Am Chem Soc. 2009; 131:12780–12791. [PubMed: 19681607]
39. Xie J, Liu G, Eden HS, Ai H, Chenm X. Surface-Engineered Magnetic Nanoparticle Platforms for Cancer Imaging and Therapy. Acc Chem Res. 2011; 44:883–892. [PubMed: 21548618]
40. Thomas CR, Ferris DP, Lee JH, Choi E, Cho MH, Kim ES, Stoddart JF, Shin JS, Cheon J, Zink JI. Noninvasive Remote-Controlled Release of Drug Molecules in Vitro Using Magnetic Actuation of Mechanized Nanoparticles. J Am Chem Soc. 2010; 132:10623–10625. [PubMed: 20681678]
41. Ruiz-Hernández E, Baeza A. Vallet-Reg, M Smart Drug Delivery through DNA/Magnetic Nanoparticle Gates. ACS Nano. 2011; 5:1259–1266. [PubMed: 21250653]
42. Xu Z, Hou Y, Sun S. Magnetic Core/Shell Fe_3O_4/Au and Fe_3O_4/Au/Ag Nanoparticles with Tunable Plasmonic Properties. J Am Chem Soc. 2007; 129:8698–8699. [PubMed: 17590000]
43. Qu Y, Cheng R, Su Q, Duan X. Plasmonic Enhancements of Photocatalytic Activity of Pt/n-Si/Ag Photodiodes Using Au/Ag Core/Shell Nanorods. J Am Chem Soc. 2011; 133:16730–16733. [PubMed: 21961900]
44. Levin CS, Hoffman C, Ali TA, Kelly AT, Morosan E, Nordlander P, Whitmire KH, Halas N. J Magnetic-Plasmonic Core-Shell Nanoparticles. ACS Nano. 2009; 3:1379–1388. [PubMed: 19441794]
45. Zhang Q, Ge J, Goebl J, Hu Y, Sun Y, Yin Y. Tailored Synthesis of Superparamagnetic Gold Nanoshells with Tunable Optical Properties. Adv Mater. 2010; 22:1905–1909. [PubMed: 20526992]
46. Lee JH, Jang TJ, Choi SJ, Moon SH, Noh SH, Kim JW, Kim JG, Park IK, Cheon J. Exchange-coupled magnetic nanoparticles for efficient heat induction. Nature Nanotechnology. 2011; 6:418–422.
47. Croissant J, Zink JI. Nanovalve-Controlled Cargo Release Activated by Plasmonic Heating. J Am Chem Soc. 2012; 134:7628–7631. [PubMed: 22540671]

48. Fan Z, Shelton M, Singh AK, Senapati D, Khan SA, Ray PC. Multifunctional Plasmonic Shell–Magnetic Core Nanoparticles for Targeted Diagnostics, Isolation, and Photothermal Destruction of Tumor Cells. ACS Nano. 2012; 6:1075–1083.
49. Schuller JA, Barnard ES, Cai W, Jun CY, White CS, Brongersma ML. Plasmonics for extreme light concentration and manipulation. Nature Materials. 2010; 9:193–204.
50. Fumagalli L, Esteban-Ferrer D, Cuervo A, Carrascosa JL, Gomila G. Label-free identification of single dielectric nanoparticles and viruses with ultraweak polarization forces. Nature Material. 2012 ASAP Article.
51. Fan K, Cao C, Pan Y, Lu D, Yang D, Feng J, Song L, Liang M, Yan X. Magnetoferritin nanoparticles for targeting and visualizing tumour tissues. Nature Nanotechnology. 2012; 7:459–464.
52. Lu W, Singh AK, Khan SA, Senapati D, Yu H, Ray PC. Gold Nano-Popcorn Based Targeted Diagonosis, Nanotherapy Treatment and In-Situ Monitoring of Photothermal Therapy Response of Prostate Cancer Cells Using Surface Enhanced Raman Spectroscopy. J Am Chem Soc. 2010; 132:18103–18114. [PubMed: 21128627]
53. Singh AK, Khan SA, Fan Z, Demeritte T, Senapati D, Kanchanapally R, Ray PC. Development of a Long-Range Surface-Enhanced Raman Spectroscopy Ruler. J Am Chem Soc. 2012; 134:8662–8669. [PubMed: 22559168]
54. Lu W, Arumugam SR, Senapati D, Singh AK, Arbneshi T, Khan SA, Yu H, Ray PC. Multifunctional Oval Shape Gold Nanoparticle Based Selective Detection of Breast Cancer Cells Using Simple Colorimetric and Highly Sensitive Two-Photon Scattering Assay. ACS Nano. 2010; 4:1739–1749. [PubMed: 20155973]
55. Liu X, Dai Q, Austin L, Coutts J, Knowles G, Zou J, Chen H, Huo Q. A OneStep Homogeneous Immunoassay for Cancer Biomarker Detection Using Gold Nanoparticle Probes Coupled with Dynamic Light Scattering. J Am Chem Soc. 2008; 130:2780–2782. [PubMed: 18257576]
56. Kumar R, Roy I, Ohulchanskky TY, Vathy LA, Bergey EJ, Sajjad M, Prasad PN. *In Vivo* Biodistribution and Clearance Studies Using Multimodal Organically Modified Silica Nanoparticles. ACS Nano. 2010; 4:699–708. [PubMed: 20088598]
57. Yezhelyev MV, Al-Hajj A, Morris C, Marcus AI, Liu T, Lewis M, Cohen C, Zrazhevskiy P, Simons JW, Rogatko A, et al. *In Situ* Molecular Profiling of Breast Cancer Biomarkers With Multicolor Quantum Dots. Adv Mater. 2007; 19:3146–3151.
58. Fang Z, Soleymani L, Pampalakis G, Yoshimoto M, Squire JA, Sargent EH, Kelley SO. Direct Profiling of Cancer Biomarkers in Tumor Tissue Using a Multiplexed Nanostructured Microelectrode Integrated Circuit. ACS Nano. 2009; 3:3207–3213. [PubMed: 19736919]
59. Song E-Q, Hu J, Wen C-Y, Tian Z-Q, Yu X, Zhang Z-L, Shi YB, Pang DW. Fluorescent-Magnetic-Biotargeting Multifunctional Nanobioprobes for Detecting and Isolating Multiple Types of Tumor Cells. ACS Nano. 2011; 5:761–770. [PubMed: 21250650]
60. Beqa L, Fan Z, Singh AK, Senapati D, Ray PC. Gold Nano-Popcorn Attached SWCNT Hybrid Nanomaterial for Targeted Diagnosis and Photothermal Therapy of Human Breast Cancer Cells. ACS Appl Mater Interfaces. 2011; 3:3316–3324. [PubMed: 21842867]
61. Nel AE, Mädle L, Velego D, Xia T, Hoek MVE, Somasundaran P, Klaessig F, Castranova nF, Thompson M. Understanding biophysicochemical interactions at the nano–bio interface. Nature Materials. 2009; 8:543–557.
62. Walczyk D, Bombelli FB, Monopoli MP, Lynch I, Dawson KA. What the Cell “Sees” in Bionanoscience. J Am Chem Soc. 2010; 132:5761–8. [PubMed: 20356039]
63. Mahmoudi M, Lynch I, Ejtehadi MR, Monopoli MP, Bombelli FB, Laurent S. Protein–Nanoparticle Interactions: Opportunities and Challenges. Chem Rev. 2011; 111:5610–5637. [PubMed: 21688848]
64. Mahmoudi M, Serpooshan V. Large protein absorptions from small changes on the surface of nanoparticles. J Phys Chem C. 2011; 11:18275–18283.
65. Mahmoudi M, Saeedi-Eslami SN, Shokrgozar MA, Azadmanesh K, Hassanlou M, Kalhor HR, Burtea C, Rothen-Rutishauser B, Laurent S, Sheibani S, Vali H. Cell “vision”: complementary factor of protein corona in nanotoxicology. Nanoscale. 2012; 4:5461–5468. [PubMed: 22842341]

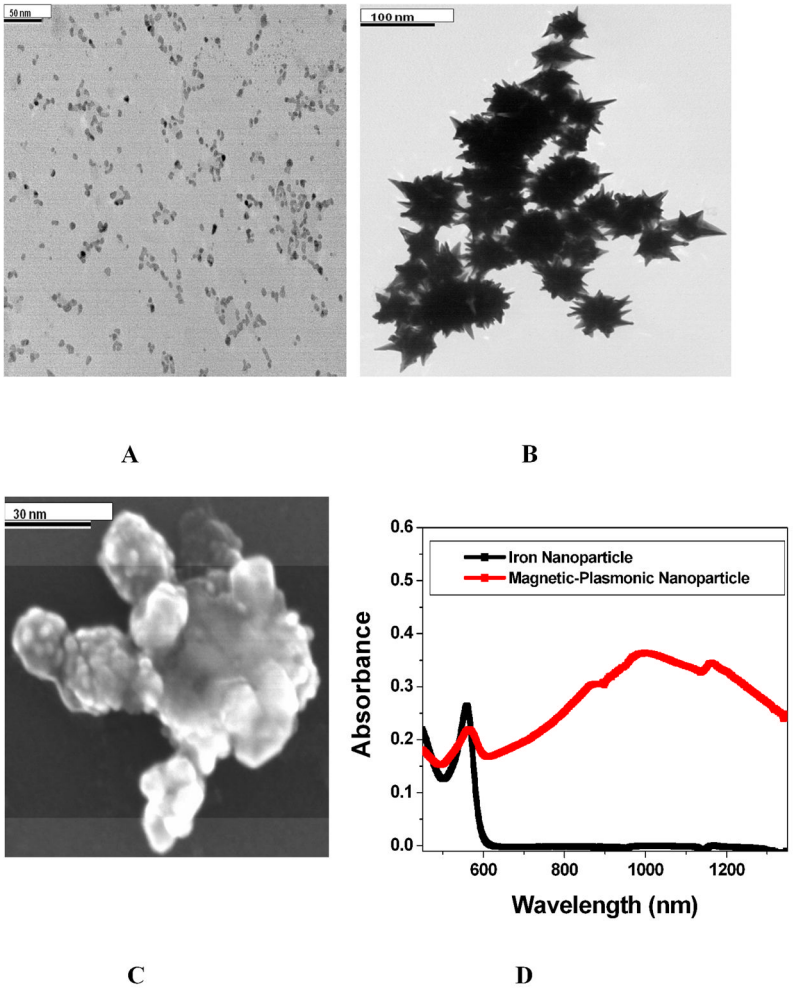

Figure 1.

A) TEM image of freshly prepared iron nanoparticle. B) TEM image of freshly prepared magnetic core-gold shell star shape nanoparticle. C) SEM images of freshly prepared magnetic core-gold shell star shape nanoparticle. D) Absorption spectra of iron nanoparticle & magnetic core-gold shell star shape nanoparticle. The strong long wavelength band in the near IR region (λ_{PR} = 1060 nm) is due to the oscillation of the conduction band electrons of gold.

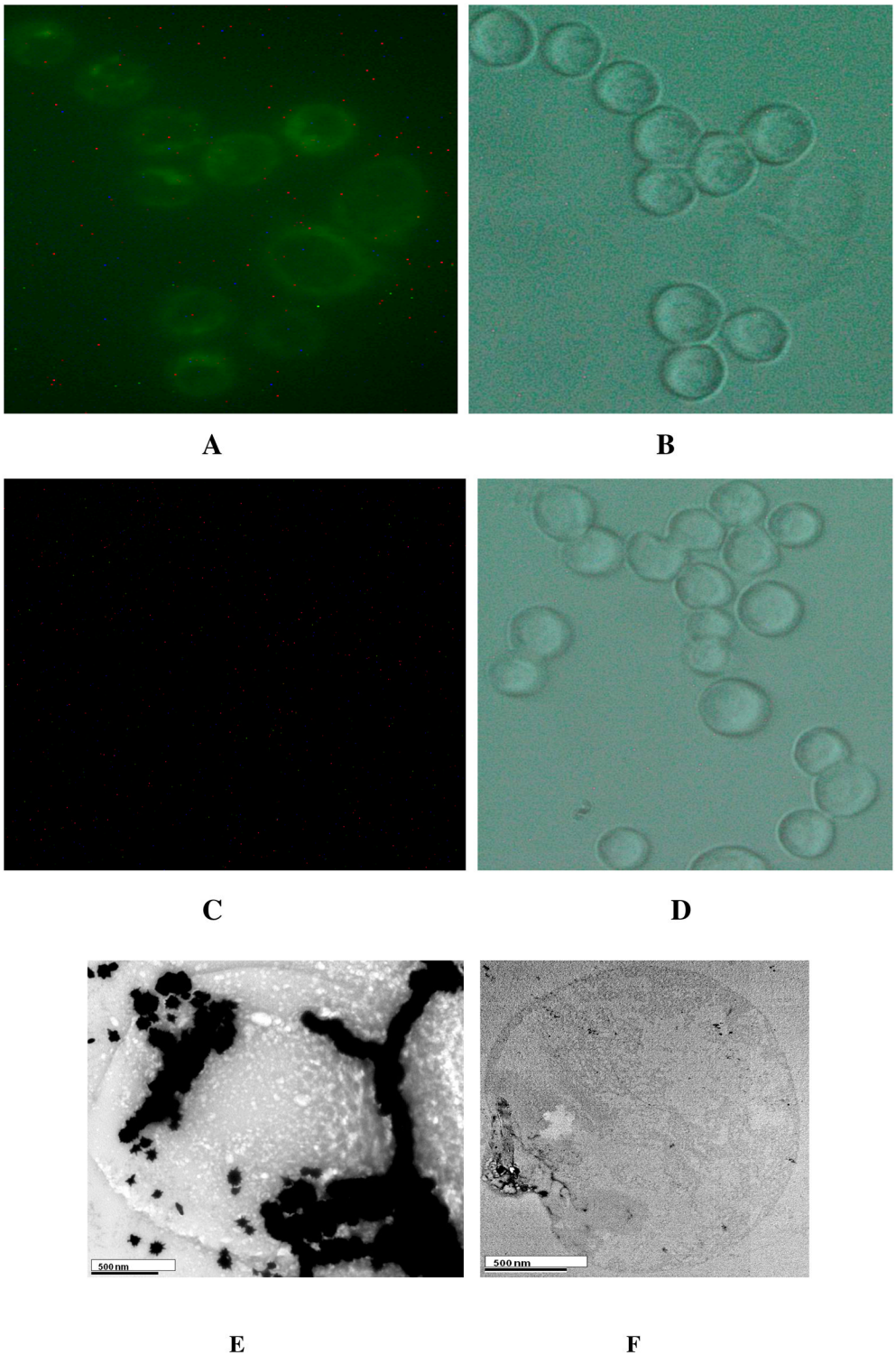

Figure 2.

(A) Fluorescent images of SK-BR-3 cancer cells after SK-BR-3 cells (1:10^5 ratio) were spiked in whole blood sample and then incubated with Cy3-modified S6 aptamer-conjugated theranostic magnetic/plasmonic nanoparticles followed by separation using a magnet. (B)

Bright-field image of the same SK-BR-3 cells after magnetic separation. (C) Blood cell fluorescent images after SK-BR-3 cells ($1:10^5$ ratio) were separated by a magnet from whole blood sample. (D) Bright-field image of the same blood cells after magnetic separation. (E) TEM image of SK-BR-3 cells after magnetic separation. The image clearly shows that Cy3-modified S6 aptamer-conjugated theranostic magnetic/plasmonic nanoparticles are attached to SK-BR-3 cells. (F) TEM image of blood cells after magnetic separation.

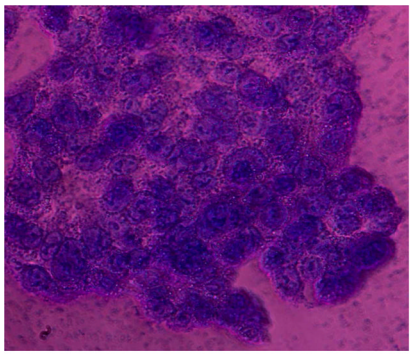

A

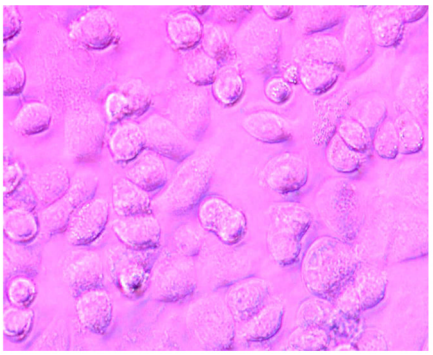

B

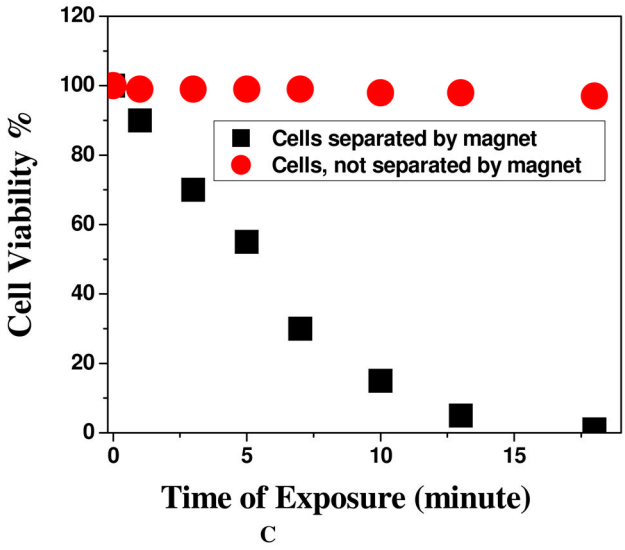

C

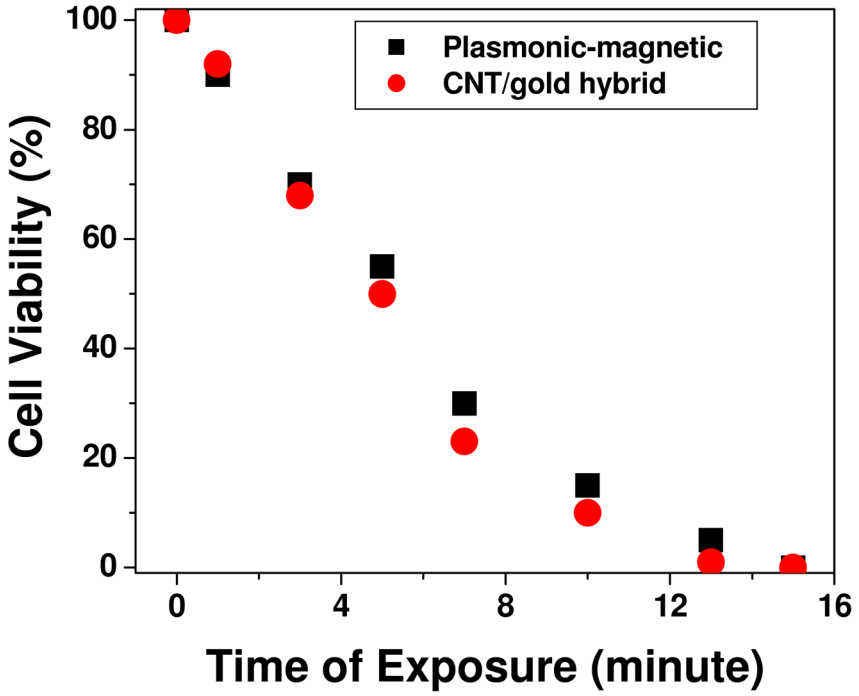

D

Figure 3.

(A) Bright-field inverted microscopic images of cells separated by the magnet and irradiated with 1064 nm near IR light at 2–3 W/cm^2 for 8 minutes followed by staining with trypan blue. (B) Bright-field inverted microscopic images of cells not separated by the magnet and irradiated with 1064 nm near IR light at 2–3 W/cm^2 for 10 minutes followed by staining with trypan blue. C) Plot showing time-dependent cell viability after irradiation with 1064 nm near IR light at 2–3 W/cm^2 for 20 minutes. D) Plot comparing photothermal therapy response between well-characterized CNT/gold hybrid and theranostic magnetic-plasmonic star shape nanoparticles when nanoparticles-conjugated SK-BR-3 cells were exposed to 1064 nm near IR light at 2–3 W/cm^2 for different times.

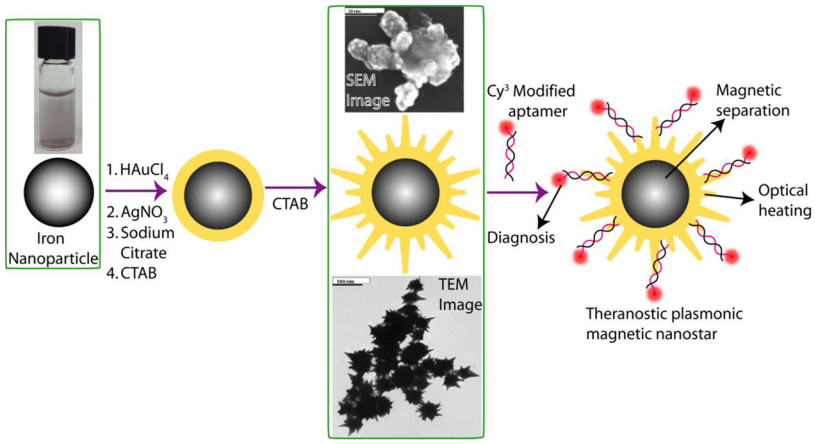

Scheme 1.

Schematic representation showing the synthesis of S6 aptamer-conjugated multifunctional theranostic magnetic core–gold shell star shape nanoparticles.

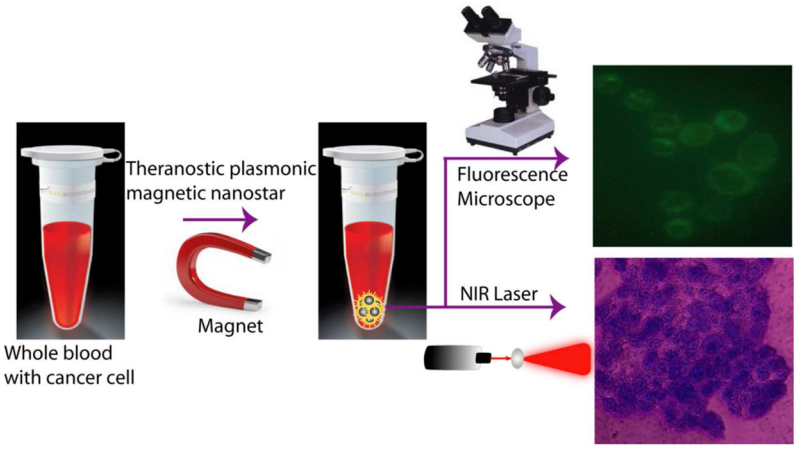

Scheme 2.

Schematic representation showing the separation of specific cancer cells using S6 aptamer-conjugated plasmonic/magnetic nanoparticles. It is then followed by the selective fluorescence imaging and targeted photothermal destruction of the specific cancer cells.